Journal Pre-proof

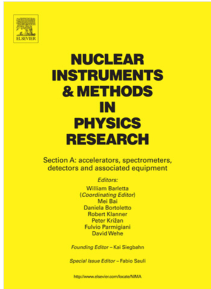

Optimal and automated mask alignment for use in edge illumination X-ray differential-phase and dark-field imaging techniques

Adam Doherty, Lorenzo Massimi, Alessandro Olivo, Marco Endrizzi

PII: S0168-9002(20)30999-2
DOI: https://doi.org/10.1016/j.nima.2020.164602
Reference: NIMA 164602

To appear in: *Nuclear Inst. and Methods in Physics Research, A*

Received date : 11 May 2020
Revised date : 12 August 2020
Accepted date : 30 August 2020

Optimal and Automated Mask Alignment for use in Edge Illumination X-Ray Differential-Phase and Dark-Field Imaging Techniques

Adam Doherty[a,*], Lorenzo Massimi[a], Alessandro Olivo[a], Marco Endrizzi[a]

[a] *Department of Medical Physics and Biomedical Engineering, University College London, London, WC1E 6BT, UK*

Abstract

Edge illumination X-ray phase-contrast imaging makes use of two absorbing masks for precise beam shaping and analysis. As the system is being translated to clinical and industrial environments, a robust quantitative algorithm is required to keep the masks precisely aligned without the need of an expert operator. We present a model for how the illumination on the detector varies as one mask is moved relative to the rest of the system. This model is based on a superposition of known illumination patterns associated with misalignment in each degree of freedom. Through inversion of this model, quantitative estimates of the degree of misalignment can be obtained, and hence can show the position of optimal alignment. The precision of alignment achievable through model inversion was tested, showing at least an order of magnitude improvement when compared to the established mask alignment procedure. Precision of the alignment along the optical axis, and around the three rotational degrees of freedom were found to be [±0.78 μm, ±0.17 *mdeg*, ±5.08 *mdeg*, ±2.39 *mdeg*] respectively, whereas the established procedure would be limited to [±42.5 μm, ±6.69 *mdeg*, ±348 *mdeg*, ±195 *mdeg*]. Furthermore, the model allows the decomposition of residuals into random and systematic components, the latter enabling accurate evaluation of imperfections in the masks' structure which have now become the main limiting factor in the final degree of alignment.

Keywords:
X-ray Dark-Field Imaging, X-ray Phase-Contrast Imaging

1. Background

Since the introduction of third-generation synchrotrons in the 1990s, there has been growing research into phase-contrast and dark-field X-ray imaging. Whereas conventional X-ray imaging achieves contrast based on X-ray absorption, phase-contrast and dark-field imaging detect angular deflections of the X-ray paths when traversing the sample. Dark-field imaging, or ultra-small angle X-ray scattering, is linked to density fluctuations on length scales below the spatial resolution of the imaging system [1] [2]. Dark-field imaging has potential applications including imaging micro-bubbles [3], defects in composite materials [4] or microfibers in ordered systems [5].

Measuring the dark-field signal requires the detection of angular deflections in the order of microradians and hence specialised setups are required for such sensitivity. We focus here on the edge illumination (EI) system due to its compact setup and compatibility with conventional X-ray sources [6] [7].

EI employs two masks on either side of the sample for modulating and analysing the radiation field (See Figure 1b for mask shape). The presence of a sample in the X-ray beam will change the intensity field at the detector through three effects: absorption, refraction and scattering. Separating these signals in an EI system requires investigating the intensity variations in each pixel as one mask is moved relative to the rest of the system. Moving one mask along the axis perpendicular to both the apertures and X-ray propagation, set as the x-axis, modulates the intensity according to what is usually called the Illumination Curve (IC). The IC is modelled as the convolution of two square apertures with an extended source and can be approximated by a Gaussian function. The sample will reduce the area under the IC due to absorption, shift the centre of the IC due to refraction and broaden the IC due to scattering. Quantifying these

EI - edge illumination, IC - Illumination Curve

*Corresponding Author
Email address: zcemado@ucl.ac.uk (Adam Doherty)

effects on a pixel-by-pixel basis results in separate images for absorption, refraction and scattering within the sample.

The approach to quantify the changes in the IC is referred to as phase retrieval and is a topic of ongoing investigation. In an ideal case, measuring the intensity at three points on the IC is sufficient [8]. In general, performing small mask movements to finely sample the IC and using an analytical fit is the most accurate approach [9], with this relative improvement in accuracy becoming increasingly more important as the dark-field signal gets weaker [10].

Reducing the number of sampling points is equivalent to fewer exposures taken during the image acquisition, and hence is key in reducing scan times. In addition, a simplified data collection requiring fewer mask movements will lead to fewer sources of error from positioning inaccuracies. It has been shown that when the masks are misaligned, only fine IC sampling can recover quantitative images [11].

If two periodic patterns are slightly mismatched, whether through translation, rotation or a change in periodicity of one pattern with respect to the other, then Moiré fringes will appear when the patterns are overlaid. The period of the fringes will increase as the patterns become more alike, and will disappear when a perfect match is found. As such, Moiré fringes are a good indicator of mask misalignment, with their shape and pitch dependent on which degrees of freedom the masks are misaligned along. However, the fringes become faint well before the masks reach the desired degree of alignment, hence visual analysis of faint fringes becomes an imprecise alignment approach. An established mask alignment procedure has been developed with an algorithm that analyses the intensity as one mask is translated to detect faint fringes, and hence is a more precise alignment approach [12].

We propose here a complete procedure, entailing data acquisition, analysis and modelling. Building upon this established alignment algorithm, we introduce a multi-Gaussian IC representation and a model of how the IC centres drift across the field of view as a function of misalignment. Through inversion of this model, we are able to calculate the physical position where the mask should be placed for optimal alignment, leading to an order of magnitude improvement in alignment precision, and hence an overall quicker alignment procedure. Moreover, the model can separate the random and systematic sources of errors, enabling a precise evaluation of the quality of the optical elements.

1.1. Edge-Illumination System

A typical EI setup is shown in Figure 1a. The system differs from the conventional X-ray setup consisting of an X-ray source, sample and detector by the introduction of two absorbing masks. The first mask is referred to as the sample mask and is placed just upstream of the sample. This mask has apertures aligned with the system y-axis and splits the beam into many beamlets, with the period between apertures denoted p_1. The second mask placed just before the detector, is aligned to cover and sharpen the pixel boundaries. When perfect alignment is reached, the period of this detector mask, p_2, is matched to that of the sample mask projected onto the plane of the detector mask. This takes into account the geometrical magnification that exists between these components, with this magnification depending on their relative positions (z_1 and z_2 in Figure 1a). Similarly, the pixel dimensions, p_3, are larger than the detector mask period in order to establish a 1-to-1 correspondence between the apertures of both masks and an individual pixel column.

Alignment of the system can be divided into the separate alignment of each of the two mask projections with a fixed detector structure. Six degrees of freedom are identified, three translation along x, y, and z, and three rotation angles around these axes, denoted θ, R and ϕ respectively. Aligning each mask is possible through coarse initial positioning by hand followed by a visual assessment of the Moiré fringes. This can achieve alignment such that all ICs peak within roughly half the mask period, but further improvement requires a more accurate analysis of the ICs in the system.

An IC scan is carried out by taking multiple exposures with no sample in place and moving one mask along the system x-axis between exposures. The IC for each pixel can be found through fitting or interpolation of the intensity measured by the pixel through the measured series of exposures.

The algorithm aims to align a mask with respect to the other elements in the system. The standard procedure entails the alignment of each mask with the detector separately, followed by refinement by keeping both masks in place.

2. Methods

The established approach to mask alignment uses a 2D plot to visualise misalignment across the field of view, which an operator can then use to judge how the mask should be adjusted to reach alignment. This 2D plot, denoted G, has entries calculated from the mask

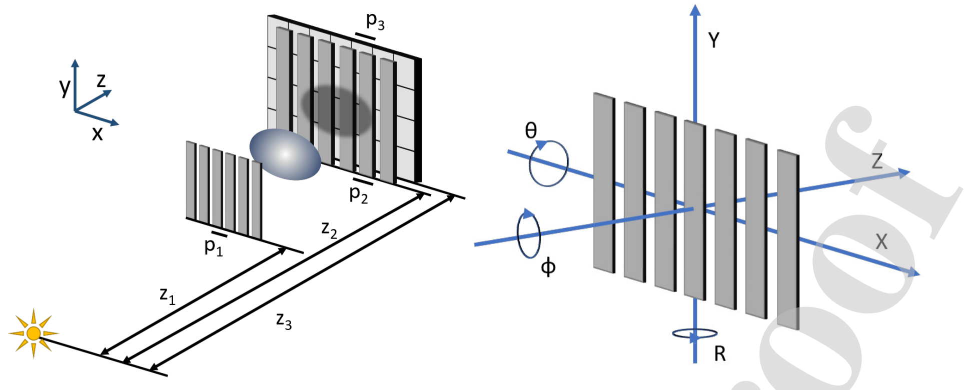

(a) (b)

Figure 1: (a) Laboratory edge illumination setup, consisting of an X-ray source, sample mask, sample, detector mask and detector. The lengths of interest when aligning the system are indicated - showing the source to masks and source to detector distances, as well as the period of both masks and the detector pixel size. (b) The 6 degrees of freedom available for mask movement, with arrows indicating movement in the positive direction.

position along the x-axis corresponding to the peak of each IC. If l is used in the following equation to denote the mask position along the x-axis during an IC scan, the entry of G for a pixel on the detector at $[X, Y]$ can be calculated as follows.

$$G(X, Y) = \arg\max_{l}[IC(X, Y, l)] \tag{1}$$

After acquiring an IC scan, the plot G is calculated by pixel-by-pixel analysis of which point on the IC resulted in the maximum intensity. There are two approaches for this, depending on how l is defined. The established method defines l which can only take discrete values based on where the IC was sampled in the IC scan. This results in a discretised stepped plot for G, which will be denoted G_{step}, with an example shown in Figure 2b.

We introduce an alternative method which is more suited to computational analysis. A Gaussian fit is used to more accurately calculate the central position of each IC, which corresponds to defining a continuous l. This results in a smooth surface, which will be denoted G_{cont}, seen in Figure 2c. This is not only a more accurate representation of the true central points on the ICs, but can also be calculated accurately with a low number of sampling points in the IC scan. From this point, G will be used to signify G_{cont} unless explicitly stated.

As the mask becomes misaligned, the ICs shift relative to one another and the range of values in G increases. How the ICs shift, and hence the shape of G, depends on which degree of freedom the mask is misaligned along.

In practice, the detector mask is rarely moved, with the sample mask moving regularly during scanning. In addition, the sample mask is much more likely to be disturbed through placing and removing samples. The result is that, in general, it is usually the sample mask which needs to be aligned. For this reason, the sample mask dimensions will be discussed from here in, but these can be switched to detector mask dimensions as necessary.

The masks are aligned when the projected period of the masks match the period of the detector. In equation form, this can be written as $Mp_1 = p_3$, where M is the magnification between the mask and detector. If instead, we start on the plane of the mask and hence start by saying $p_1 = \frac{p_3}{M}$. However, if there is a misalignment along the z-axis, this equation will not hold and instead, the following equation defines the projection mismatch.

$$\frac{p_3}{M'} - p_1 = \delta\mu \tag{2}$$

Where M' symbolises the mismatched magnification, $\frac{z_3}{z_1 + z}$, with z being the mask misalignment. The term $\delta\mu$ is the shift in the centre of two neighbouring ICs along the x-dimension of the mask. Inserting the explicit form of M' and rearranging gives the following.

$$z = z_1 \frac{\delta\mu}{p_1} \tag{3}$$

$$z = z_1 a_z \tag{4}$$

The final step recognises that the fraction $\frac{\delta\mu}{p_1}$ is equal to the gradient along the x-dimension of G, and has been replaced by a coefficient showing that this is can be defined as a feature of G related to misalignment along the z-axis.

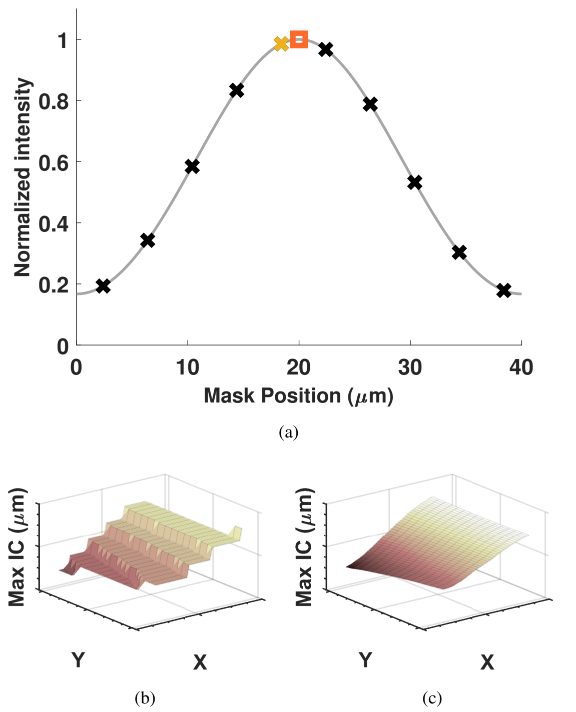

Figure 2: (a) The IC for a pixel with points showing the calculation for the corresponding element of G. The raw data from 10 exposures as the mask is moved by $40\mu m$ is shown as crosses, with a Gaussian fit passing through the points. (b) G_{step} is obtained when each entry is set as the mask position along x which resulted in maximum exposure in the pixel, shown as the yellow cross above. (c) G_{cont} when each entry is calculated after fitting a function to the data, with an accurate guess for the central point on the IC shown as the orange square.

The equivalent equation for the misalignment in ϕ benefits from having no reliance on the magnification, and would apply for a parallel beam system. If the equivalent gradient along the y-dimension of G is expressed as a_ϕ, then this gradient can be seen as the tangent of the misalignment angle ϕ.

$$\tan\phi = -a_\phi \tag{5}$$

For θ misalignment, the equation for misalignment in z can show the relative shift along z between the top and bottom of the mask. If we define a new parameter a_θ equivalent to a constant second order gradient $\frac{\partial}{\partial y}\frac{\partial G}{\partial x}$, then the following equation can calculate the misalignment along θ.

$$\sin\theta = z_1 a_\theta \tag{6}$$

This same principle can be used to calculate misalignment in R. A coefficient a_R is defined as $\frac{\partial^2 G}{\partial x^2}$, leading to the final equation from converting from model parameters to misalignment in real space.

$$\sin R = z_1 a_R \tag{7}$$

In the established mask alignment procedure, each degree of freedom would be aligned one-by-one by removing their known features that appear with misalignment. Aligning each degree of freedom takes multiple iterations of IC scans and mask adjustments, with each mask movement up to the judgement of the operator. This becomes more difficult if misalignment is strong in all degrees of freedom, which will in general mean that after the first attempt at aligning all degrees of freedom individually, this procedure would be repeated at least once to reach optimal alignment.

This procedure comes with two major issues. The first is the lack of knowledge on quantitative mask adjustments means that multiple iterations are required to align a single degree of freedom. After proceeding through all degrees of freedom, and then repeating this process, it would be common that tens of IC scan plus mask adjustment iterations have been carried out, with this number dependent on the skill of the operator.

The second major fault is the lack of precision in the final alignment. The plot G_{step} will appear flat if all ICs peak within the sampling period of an IC scan, which is generally on a scale of a few microns. Considering the shifts in IC positions due to sample refraction in phase-contrast imaging are on a similar scale, this precision in alignment is very large. The mask can be more accurately aligned through plotting G_{step} either side of perfect alignment and extracting an optimal position, however, this further increases the number of iterations to reach alignment, and again is operator dependent.

2.1. Model

The known features that appear in G when the mask is misaligned can indicate the degree of misalignment. Modelling these features as the basis shown in Figure 3 allows representing G as a superposition of surfaces, each associated with misalignment in one specific degree of freedom. These surfaces can be defined as the following:

$$S_z = X \quad S_\phi = Y \quad S_\theta = XY \quad S_R = XX \tag{8}$$

Where X is an array containing the x-coordinate of each entry associated with each pixel, with Y a similar array for the y-coordinates. These arrays can be calculated from the mask period and number of apertures, with the central element defined with coordinates (0,0). The plot G is defined on the plane of the mask being aligned, so

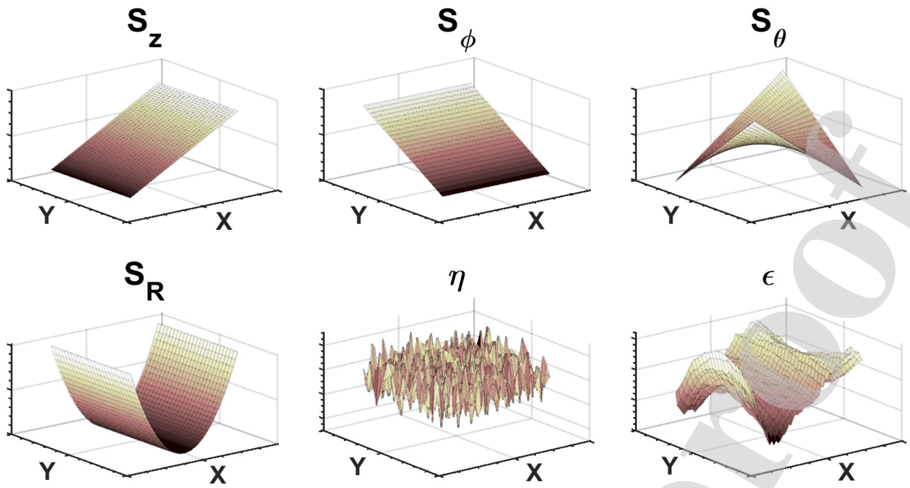

Figure 3: Using the model equation for G (Equation 9), any plot can be decomposed into a series of surfaces. The surfaces with shapes S_z, S_ϕ, S_θ, S_R contribute more strongly as the mask becomes more misaligned along each corresponding degree of freedom, with the final two terms corresponding to random and systematic noise respectively.

the range in values in X and Y are the spatial dimensions of the mask within the field of view.

In addition to the four surfaces described above, three terms are introduced to represent a baseline as well as the random and the systematic noise (represented as a_0, η and ϵ respectively). The baseline corresponds to the mask alignment along the x-axis, which can be neglected in this alignment algorithm. The contribution of each misalignment surface is determined by four scalar coefficients seen earlier in Equations 4-7. Using this model, a least-squares solver can extract the four coefficients of interest, quantifying misalignment along each degree of freedom. The model for G can be expressed as the following equation:

$$G = a_0 + a_z S_z + a_\phi S_\phi + a_\theta S_\theta + a_R S_R + \eta + \epsilon \qquad (9)$$

The final step is using Equations 4-7 to find the mask position in real space, and hence move the mask to a predicted position of optimal alignment.

Phase wrapping can occur when the mask is misaligned and is unavoidable when the degree of misalignment is relatively large. This is when there is not a 1-to-1 correspondence between apertures and pixels, or the IC scan is initiated towards the peaks of most ICs rather than their minima. When phase wrapping occurs, the surfaces are incorrectly fit, and the mask position is incorrectly estimated (Figure 4a). In general, unwrapping can correct the plot (Figure 4b), by finding large discontinuities and correcting by the addition or subtraction of the mask period. If phase wrapping is corrected for then the algorithm can work after only coarse initial positioning by hand, relaxing the need to remove Moiré fringes.

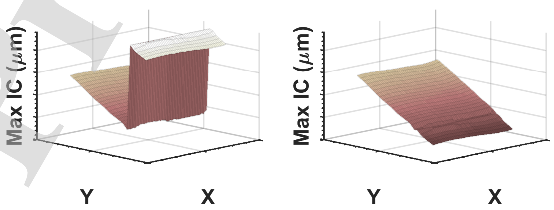

(a) (b)

Figure 4: (a) Resulting plot for G when strong misalignment in ϕ leads to phase wrapping. (b) Corrected surface after adjusting for large discontinuities.

2.2. Validation

To validate the model, several IC scans were taken with two different mask sets and varying the degrees of misalignment. All scans were taken on the same system, which consisted of a Rigaku MM007 rotating anode tube (Rigaku Corporation, Japan) with a Molybdenum anode and an effective focal spot size of approximately 70 μm and a CMOS-based flat-panel C9732DK-11 (Hamamatsu, Japan) with a pixel size of 50 x 50 μm^2. A line-skipping setup was used [13], meaning every other pixel column would be aligned to a mask aperture, resulting in effective pixel sizes of 50 x 100 μm^2. The masks were manufactured to the Authors' design by Microworks GmbH, Karlsruhe, Germany. For the sample mask motors, Newport linear stages were used for mask translation, with models ILS150PP for translation along the x-axis and MFA-CC for translation along z. Sample mask rotation through *R* was using a Newport SR50CC. Goniometer stages from Kohzu Precision were used for the other rotation axis, with model SA070-RM-R used for rotation through ϕ and θ.

An IDL script was used to control the system for data acquisition and on-line analysis for calculating the position of optimum alignment. This analysis was carried out by an algorithm based on the model defined in Section 2.1.

The first dataset used for validation used masks consisting of gold deposited on a graphite substrate. The sample mask had a period of 79 μm and was placed roughly 65 cm from the source. The detector mask had a larger period of 98 μm and was placed just in front of the detector roughly 85 cm from the source. This dataset was used to validate the accuracy of the algorithm, through observing the estimated mask position as the mask was moved along all degrees of freedom separately.

The second dataset used a different set of masks, with gold deposited on a silicon substrate. The period of the masks were 49 μm and 61 μm for the sample mask and detector mask respectively. Their distances from the source were the same as before, however, the detector would now be moved to 1.4 m from the source to match every other pixel column to an aperture. This dataset was primarily used as a statistical analysis of the noise seen in repeated IC scans.

3. Results and Discussion

The validity of the algorithm was shown by comparing the estimated mask position to the true mask position as the sample mask is moved to different positions in all degrees of freedom. A comparison between the algorithm estimates and the true mask movements is presented in Figure 5. The algorithm follows the mask movement well, with small deviations arising from some coupling between different degrees of freedom. These plots show that the proposed algorithm is accurate in identifying the correct mask position over a wide range of misalignments.

The true mask position is defined relative to a previously aligned system, with this position set as zero, with known displacements given using motors to translate or rotate the mask. This means a small systematic error is present due to the imperfect calibration to zero achieved by using the established procedure, and further statistical errors arising from motor movement errors. However, both of these errors can be ignored on the scale of Figure 5, with no quantitative results deduced from this data.

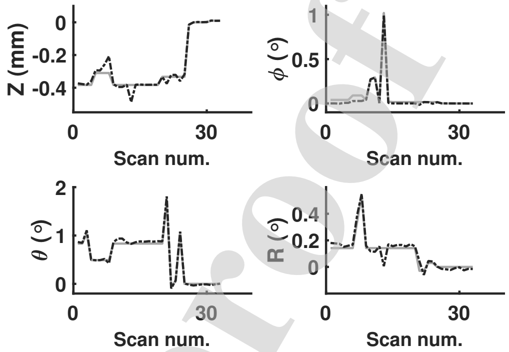

Figure 5: The true mask position shown as a solid line compared to the estimated mask position as a dotted line for 33 different IC scans. The larger discrepancies are due to coupling of the degrees of freedom which were are not perfectly captured by the model.

High precision in the estimated mask position will mean fewer iterations are required to reach alignment. This is quantified through repeating IC scans at the same mask positions, with the standard deviation of the estimated mask position in each degree of freedom used to quantify precision. Two positions were chosen to take repeated measurements. Position 1 is the mask at near alignment, while position 2 is at a misalignment where weak Moiré fringes are visible. The mean position of mask at position 1 was [13.1 μm, 0.97 *mdeg*, 25.6 *mdeg*, -128 *mdeg*] along [z, ϕ, θ, *R*] respectively, and at position 2 was [-133 μm, -25.0 *mdeg*, -309 *mdeg*, -131 *mdeg*]. The standard deviations in the estimated mask positions from 30 scans at each position are shown in Table 1.

	z (μm)	ϕ(*mdeg*)	θ(*mdeg*)	R (*mdeg*)
Pos 1	±0.33	±0.11	±1.31	±2.55
Pos 2	±0.78	±0.17	±5.08	±2.39

Table 1: The precision in each degree of freedom from repeated scans of the mask at two different positions. The precision of the new algorithm was calculated using the standard deviation of the 30 estimates of the mask position from 30 different IC scans.

The precision using the established procedure is limited by the sampling rate in the IC scans. Equivalent estimates to those in Table 1 for the precision along each degree of freedom can be calculated using equations for the alignment tolerance [12]. Using the IC sampling period of 3.27 μm, the precision in using the established procedure would be [±42.5 μm, ±6.69 *mdeg*,

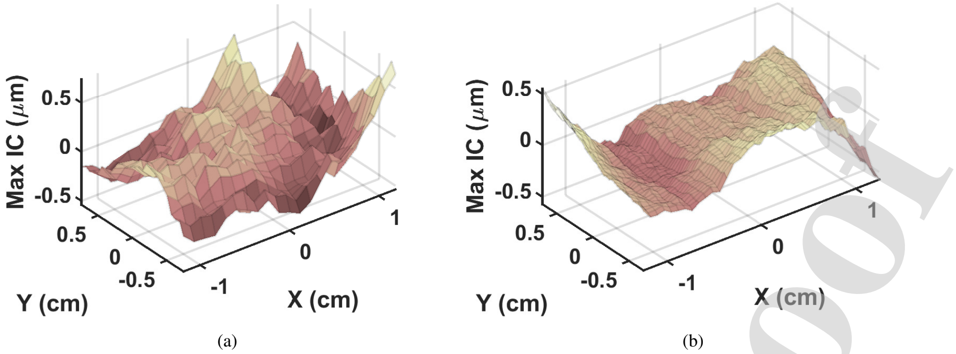

Figure 6: Systematic error visualised across the two different masks setups over a field of view of 1.5 x 2.5 cm on the sample masks. (a) Shows the set of graphite substrate masks with 79 μm sample mask period and (b) shows the Silicon substrate masks with 49 μm sample mask period.

± 348 *mdeg*, ± 195 *mdeg*]. The new approach presented sees an improvement of at least one order of magnitude in each degree of freedom.

This vast improvement in precision is due to both the accurate fitting of the IC data, rather than calculating G using the exposure resulting in maximum intensity, and to the inversion of the model which provides directly the position of optimum alignment. Whereas previously the central position of the IC is only known with uncertainty of the IC sampling period of 3.27 μm, repeated IC scans show that this central position is estimated using the Gaussian fit approach with an uncertainty of a few tens of nanometers.

The increased precision means that the final alignment is now limited by the systematic noise in G. Using the proposed model, one can remove all features in G from misalignment and remove all random noise through averaging, leaving a visualisation of the systematic noise, ϵ. This systematic noise is believed to be the result of the combination of the imperfections of the sample and detector masks. Figure 6 show the systematic noise on central regions of the two different mask setups. Roughly the same field of view of 1.5 x 2.5 cm is shown in these plots. Both figures show the systematic error on the scale of ± 0.5 μm, which is smaller than the IC sampling period (± 2.63 μm and ± 1.63 μm for graphite substrate and Silicon substrate masks respectively), but larger than the random noise of a few tens of nanometers.

These results were observed using an IC sampling typically used for the established procedure. However, we note that the Gaussian fitting process in calculating G may allow fewer sampling points and hence faster data acquisition. A further increase in speed is provided by reducing the number of iterations to reach alignment, which will arguably be of greater importance. With the proposed algorithm only a few (3 to 4) iterations are needed to account for the practical problems of noise and coupling between axes. The model assumes that the axes of rotation all pass through the centre pixel of the mask, as shown in Figure 1b. If the actual positioner arrangements do not allow for the centre of the system of reference to match the centre of the mask the result, in practice, is that these degrees of freedom are coupled. In summary, the quantitative nature of the new procedure enables the system to be aligned much quicker, with the precision in the final alignment much improved than previously.

4. Conclusion

Strict mask alignment in an edge illumination X-ray imaging setup allows for faster imaging. The established mask alignment procedure requires a user to assess the uniformity of a 2D surface plot and involves iterating between scanning the masks and moving them to a new estimate of a better alignment position. The basis for the new alignment algorithm presented is a model that decomposes the surface plot into known shapes associated with misalignment along each degree of freedom, with derived equations enabling the inversion of the model coefficients into an estimate of the mask position in real space. This enables alignment to be reached in fewer iterations and removes the need for an experienced user. The model also allows the combined imperfections in the two masks to be visualised across the field of view, which can provide feedback on the fabrication of the mask and mounting towards improvement on both these fronts. Validation has shown that an improvement on alignment precision in excess of one order of magnitude, and that it is the mask imperfections that are now limiting the uniformity of the illumination on the detector.

5. Acknowledgements

This work is supported by EPSRC (EP/R513143/1, EP/T005408/1). ME was supported by the Royal Academy of Engineering under the RAEng Research Fellowships scheme. AO was supported by the Royal Academy of Engineering under the Chairs in Emerging Technologies scheme.

References

[1] L. Rigon, H.-J. Besch, F. Arfelli, R.-H. Menk, G. Heitner, H. Plothow-Besch, A new DEI algorithm capable of investigating sub-pixel structures, Journal of Physics D: Applied Physics 36 (10A) (2003) A107–A112. doi:10.1088/0022-3727/36/10A/322.

[2] T. E. Gureyev, S. W. Wilkins, Regimes of X-ray phase-contrast imaging with perfect crystals, Nuovo Cimento della Società Italiana di Fisica D - Condensed Matter, Atomic, Molecular and Chemical Physics, Biophysics 19 (2-4) (1997) 545–552. doi:10.1007/BF03041015.

[3] T. P. Millard, M. Endrizzi, N. Everdell, L. Rigon, F. Arfelli, R. H. Menk, E. Stride, A. Olivo, Evaluation of microbubble contrast agents for dynamic imaging with x-ray phase contrast, Scientific Reports 5 (2015) 12509. doi:10.1038/srep12509.

[4] P. Fromme, M. Endrizzi, A. Olivo, Defect imaging in composite structures, in: AIP Conference Proceedings, Vol. 1949, AIP Publishing LLC, 2018, p. 130004. doi:10.1063/1.5031599.

[5] V. Revol, B. Plank, R. Kaufmann, J. Kastner, C. Kottler, A. Neels, Laminate fibre structure characterisation of carbon fibre-reinforced polymers by X-ray scatter dark field imaging with a grating interferometer, NDT & E International 58 (2013) 64–71. doi:10.1016/J.NDTEINT.2013.04.012.

[6] A. Olivo, R. Speller, A coded-aperture technique allowing x-ray phase contrast imaging with conventional sources, Applied Physics Letters 91 (7) (2007) 074106. doi:10.1063/1.2772193.

[7] G. Havariyoun, F. A. Vittoria, C. K. Hagen, D. Basta, G. K. Kallon, M. Endrizzi, L. Massimi, P. Munro, S. Hawker, B. Smit, A. Astolfo, O. J. Larkin, R. M. Waltham, Z. Shah, S. W. Duffy, R. L. Nelan, A. Peel, T. Suaris, J. L. Jones, I. G. Haig, D. Bate, A. Olivo, A compact system for intraoperative specimen imaging based on edge illumination x-ray phase contrast, Physics in Medicine & Biology 64 (23) (2019) 235005. doi:10.1088/1361-6560/ab4912.

[8] M. Endrizzi, P. C. Diemoz, T. P. Millard, J. Louise Jones, R. D. Speller, I. K. Robinson, A. Olivo, Hard X-ray dark-field imaging with incoherent sample illumination, Applied Physics Letters 104 (2) (2014) 024106. doi:10.1063/1.4861855.

[9] A. Astolfo, M. Endrizzi, G. Kallon, T. P. Millard, F. A. Vittoria, A. Olivo, A first investigation of accuracy, precision and sensitivity of phase-based x-ray dark-field imaging, Journal of Physics D: Applied Physics 49 (48) (2016) 485501. doi:10.1088/0022-3727/49/48/485501.

[10] C. J. Maughan Jones, F. A. Vittoria, A. Olivo, M. Endrizzi, P. R. T. Munro, Retrieval of weak x-ray scattering using edge illumination, Optics Letters 43 (16) (2018) 3874. doi:10.1364/OL.43.003874.

[11] M. Endrizzi, D. Basta, A. Olivo, Laboratory-based X-ray phase-contrast imaging with misaligned optical elements, Applied Physics Letters 107 (12) (2015) 124103.

[12] T. P. Millard, M. Endrizzi, K. Ignatyev, C. K. Hagen, P. R. T. Munro, R. D. Speller, A. Olivo, Method for automatization of the alignment of a laboratory based x-ray phase contrast edge illumination system, Review of Scientific Instruments 84 (8) (2013) 083702. doi:10.1063/1.4816827.

[13] K. Ignatyev, P. R. Munro, R. D. Speller, A. Olivo, Effects of signal diffusion on x-ray phase contrast images, Review of Scientific Instruments 82 (7) (2011) 073702. doi:10.1063/1.3606442.

Ms. Ref. No.: NIMA-D-20-00467
Title: Optimal and Automated Mask Alignment for use in Edge Illumination X-Ray Differential-Phase and Dark-Field Imaging Techniques
Nuclear Inst. and Methods in Physics Research, A

Credit Author Statement

Adam Doherty: Conceptualization, Methodology, Software, Validation, Formal analysis, Investigation, Writing - Original Draft, Visualization

Lorenzo Massimi: Conceptualization, Methodology, Investigation, Writing - Review & Editing

Alessandro Olivo: Conceptualization, Writing - Review & Editing, Supervision

Marco Endrizzi: Conceptualization, Methodology, Software, Writing - Review & Editing, Supervision

Declaration of interests

☒ The authors declare that they have no known competing financial interests or personal relationships that could have appeared to influence the work reported in this paper.

☐The authors declare the following financial interests/personal relationships which may be considered as potential competing interests: